

Evolution of spin density vectors in a strongly focused composite field

Xiaoyan Pang (庞晓炎)^{1*}, Chen Feng (冯晨)¹, and Xinying Zhao (赵馨颖)^{2**}

¹School of Electronics and Information, Northwestern Polytechnical University, Xi'an 710072, China

²School of Physics & Information Technology, Shaanxi Normal University, Xi'an 710061, China

*Corresponding author: xypan@nwpu.edu.cn

**Corresponding author: zhaoxinyingxy@163.com

Received August 31, 2020 | Accepted September 11, 2020 | Posted Online December 10, 2020

The evolution of the spin density vectors (SDVs) is studied in a strongly focused composite field. It is found that the SDVs can be spiral along the propagation axis, and they are perpendicular to the y_s direction on the y_s axis. This behavior is governed by the Gouy phase difference between the field polarization components. The 60° rotation of the spatial distribution of the transverse SDVs is also generated, which is found to be controlled by the Gouy phase difference between the field orbital angular momentum modes. Additionally, the spin density singularities are observed in the evolution of the SDVs.

Keywords: spin density; Gouy phase; orbital angular momentum; spin angular momentum; polarization.

DOI: [10.3788/COL202119.022601](https://doi.org/10.3788/COL202119.022601)

1. Introduction

Maybe the most typical quantity for characterizing three-dimensional (3D) optical vector fields is the spin (angular momentum) density vector (SDV), whose direction represents the orientation of the polarization ellipse, and the scale indicates the density of the spin angular momentum^[1,2]. Since its important role in 3D nano-optics, for instance, in controlling light-matter interaction^[3] and in the emission directivity of a dipole-like nano-particle^[4], the SDV has attracted much attention in recent years^[5–14]. It has been found that transverse spin density (SD) has a strong connection with the spin Hall effect of light^[5,6], and the purely transverse SDVs (tSDVs) lead to an interesting optical phenomenon—the ‘photonic wheel’^[7–9]; furthermore, the spiral behavior of the SDVs provides a new rotation freedom in optical tweezers^[10–12]. The new features of SDVs continue to be observed^[13,14].

The Gouy phase is an additional phase that the focused field acquires, compared to an ideal non-diffracted field^[15–17], and it plays a fundamental role in many applications, like in terahertz spectroscopy^[18] and optical calibration^[19,20]. Because of the polarization effect in strongly focused fields, there will be a Gouy phase difference between the field components with different polarizations^[20]. It has been found that this Gouy phase difference leads to the rotation of the SDVs during beam propagation^[10–12]. The vortex beams with different orbital angular momentum (OAM) modes (i.e., different topological charges) have been studied substantially in past decades^[21–27], and it has been demonstrated that the (accumulated) Gouy phase

difference between the beams with different OAM modes can induce the rotation of the field distributions^[21,22]. Then, it will be of interest to examine the behaviors of the SDVs in a field with two distinguishing Gouy phase differences. Additionally, it is shown that in 3D optical fields, new types of optical singularities can exist: the SD singularities^[14], and these new singularities also have an effect on the behavior of the SDVs.

In this Letter, we compose a simple 3D field where two types of Gouy phase differences (i.e., the difference between the field polarization components and the difference between the field OAM modes) exist. It will be shown that the evolution of SDVs in such a 3D field is strongly dependent on these two Gouy phase differences. Also, as it will be seen, in the evolution of the SDVs, the SDV singularities can be observed, and their effect on the SDVs will be discussed.

2. Strongly Focused Composite Field

Suppose that there are two vortex Gaussian beams with topological charges $t_1 = +1$ and $t_2 = -2$, and these two beams are superimposed collinearly. Then, the complex amplitude of the composite electric field at the beam waist w_0 can be expressed as^[28]

$$E_0(r, \phi) = e^{-r^2/w_0^2} r (Ae^{i\phi} + Be^{-i2\phi}), \quad (1)$$

where (r, ϕ) are polar coordinates in the transverse plane ($x = r \cos \phi, y = r \sin \phi$), and A, B are measures of the amplitudes

of the two beams. The intensity and the phase distribution of this composite field are shown in Fig. 1, where $A = B$. In Fig. 1(a), the intensity is normalized to its maximum at the waist plane. It is shown that the intensity of the composite field has three lobes, and, when the difference between A and B is increased, these lobes will be blurred. The white lines in Fig. 1(b) indicate the phase singularities, and the phases across the white line have a π phase jump.

Now, assume that this composite beam [Eq. (1)] is linearly polarized in the x direction and is also incident upon a strongly focused system with the entrance plane coincident with the waist plane of the composite beam. The strongly focused system is illustrated by Fig. 2, where the focal length is f , and a semi-aperture angle is denoted by α . By applying the Richards–Wolf vectorial diffraction theory^[29], we can calculate the electric field of the strongly focused composite field in the focal region at point (ρ_s, ϕ_s, z_s) as [note that the following equations can be calculated by putting Eq. (1) as the incident field into Eq. (2) of Ref. [20] or referring to the derivation of Eq. (2.26) in Ref. [29]]

$$\mathbf{E}(\rho_s, \phi_s, z_s) = \hat{x}e_x + \hat{y}e_y + \hat{z}e_z, \quad (2)$$

and

$$e_x(\rho_s, \phi_s, z_s) = -ik \int_0^\alpha P(\theta, z_s) (I_{x0} + I_{x1} + I_{x2} + I_{x3} + I_{x4}) d\theta, \quad (3)$$

$$e_y(\rho_s, \phi_s, z_s) = -ik \int_0^\alpha P(\theta, z_s) (I_{y0} + I_{y1} + I_{y3} + I_{y4}) d\theta, \quad (4)$$

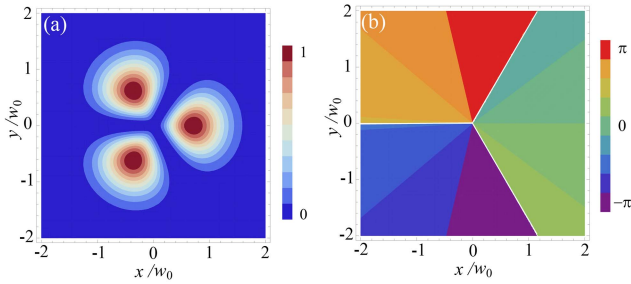


Fig. 1. Intensity and phase distribution of the incident field at the waist plane. (a) Intensity, (b) phase. Here, $A = B$.

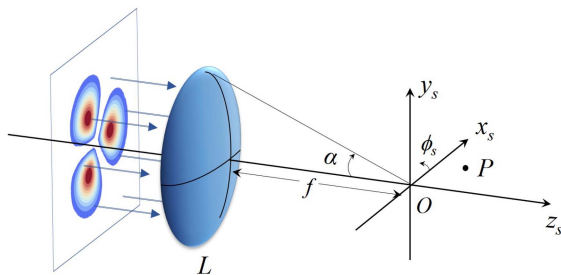


Fig. 2. Schematic illustration of a strongly focusing system. The origin O of the coordinate system is taken at the geometrical focus.

$$e_z(\rho_s, \phi_s, z_s) = -ik \int_0^\alpha P(\theta, z_s) (I_{z0} + I_{z1} + I_{z2} + I_{z3}) d\theta, \quad (5)$$

where

$$P(\theta, z_s) = \sqrt{\cos \theta} (f \sin \theta)^2 e^{-(f \sin \theta)^2 / w_0^2} e^{ikz_s \cos \theta}, \quad (6)$$

and

$$I_{x0}(\theta; \rho_s, \phi_s) = -\frac{1}{4} B (1 - \cos \theta) J_0(k\rho_s \sin \theta), \quad (7)$$

$$I_{x1}(\theta; \rho_s, \phi_s) = i\frac{1}{2} A \left[(1 + \cos \theta) e^{i\phi_s} - \frac{1}{2} (1 - \cos \theta) e^{-i\phi_s} \right] \times J_1(k\rho_s \sin \theta), \quad (8)$$

$$I_{x2}(\theta; \rho_s, \phi_s) = -\frac{1}{2} B (1 + \cos \theta) e^{-i2\phi_s} J_2(k\rho_s \sin \theta), \quad (9)$$

$$I_{x3}(\theta; \rho_s, \phi_s) = i\frac{1}{4} A (1 - \cos \theta) e^{i3\phi_s} J_3(k\rho_s \sin \theta), \quad (10)$$

$$I_{x4}(\theta; \rho_s, \phi_s) = -\frac{1}{4} B (1 - \cos \theta) e^{-i4\phi_s} J_4(k\rho_s \sin \theta), \quad (11)$$

$$I_{y0}(\theta; \rho_s, \phi_s) = i\frac{1}{4} B (1 - \cos \theta) J_0(k\rho_s \sin \theta), \quad (12)$$

$$I_{y1}(\theta; \rho_s, \phi_s) = \frac{1}{4} A (1 - \cos \theta) e^{-i\phi_s} J_1(k\rho_s \sin \theta), \quad (13)$$

$$I_{y3}(\theta; \rho_s, \phi_s) = \frac{1}{4} A (1 - \cos \theta) e^{i3\phi_s} J_3(k\rho_s \sin \theta), \quad (14)$$

$$I_{y4}(\theta; \rho_s, \phi_s) = -i\frac{1}{4} B (1 - \cos \theta) e^{-i4\phi_s} J_4(k\rho_s \sin \theta), \quad (15)$$

$$I_{z0}(\theta; \rho_s, \phi_s) = -\frac{1}{2} A \sin \theta J_0(k\rho_s \sin \theta), \quad (16)$$

$$I_{z1}(\theta; \rho_s, \phi_s) = -i\frac{1}{2} B \sin \theta e^{-i\phi_s} J_1(k\rho_s \sin \theta), \quad (17)$$

$$I_{z2}(\theta; \rho_s, \phi_s) = \frac{1}{2} A \sin \theta e^{i2\phi_s} J_2(k\rho_s \sin \theta), \quad (18)$$

$$I_{z3}(\theta; \rho_s, \phi_s) = i\frac{1}{2} B \sin \theta e^{-i3\phi_s} J_3(k\rho_s \sin \theta), \quad (19)$$

where $k = 2\pi/\lambda$ is wave number, and $J_n(x)$ is the n^{th} -order Bessel function of first kind. We can see that there are three field (polarization) components with different expressions in the focal region.

3. Evolution of SDVs

Before examining the behavior of the SDVs in this focused field, we will first review some related concepts.

The Gouy phase is a physical quantity to measure the phase difference between the actual field and the non-diffracted (ideal) field in the same conditions^[15], and, in a strongly focused field, a Gouy phase δ_i of the field component e_i can be written as

$$\delta_i(\rho_s, \phi_s, z_s) = \text{Arg}[e_i] - kR, \quad i = x, y, z, \quad (20)$$

where Arg means the phase of the field component, and $R = \sqrt{\rho_s^2 + z_s^2}$ is the distance of the point from the focus. For a laser mode, the Gouy phase is usually used to represent the accumulated phase difference of the whole beam, i.e., the ‘general’ Gouy phase, and, in that case, the Gouy phase (δ_g) of a Laguerre–Gaussian (LG) beam with topological charge t and radial mode p is given by^[21,22]

$$\delta_g(z_s) = (2p + |t| + 1) \arctan(z_s/z_R), \quad (21)$$

where z_R means the Rayleigh range. Generally speaking, the Gouy phase δ_g reflects the extra phase that the beam acquires after propagating through the focus, and, under the paraxial approximation, δ_g in Eq. (21) and δ_i in Eq. (20) are essentially the same. In order to avoid confusion, from here on, we call the Gouy phase of the whole beam as the ‘general Gouy phase.’ If the beam is singly ringed ($p=0$), and the general Gouy phase is cumulated from $z_s = -\infty$ to $z_s = +\infty$, the δ_g equals $(|t| + 1)\pi$.

The SDV, \mathbf{s}_E of the electric field, according to its definition^[1,2] and Eq. (20), in the present 3D field can be expressed by the Gouy phase difference $\delta_{ij} = \delta_i - \delta_j$ ($i, j = x, y, z$)^[2,9,10] as

$$\mathbf{s}_E = \frac{\epsilon_0}{4\omega} \text{Im}(\mathbf{E}^* \times \mathbf{E}) = \begin{pmatrix} \mathbf{s}_E^{(x)} \\ \mathbf{s}_E^{(y)} \\ \mathbf{s}_E^{(z)} \end{pmatrix} = \frac{\epsilon_0}{2\omega} \begin{pmatrix} |e_y||e_z| \sin \delta_{yz} \\ |e_x||e_z| \sin \delta_{xz} \\ |e_x||e_y| \sin \delta_{yx} \end{pmatrix}, \quad (22)$$

where ϵ_0 denotes the permittivity of free space, and ω is the angular frequency. Im and $*$ represent the imaginary part and the complex conjugate, respectively.

In the following, the evolution of SDVs in the focal region of this strongly focused composite field is discussed. Note that in this Letter only the case of $A = B$ is considered.

First, the SDVs can spin along the propagation axis (i.e., z_s axis). From Eqs. (3)–(19), one can find that when $\rho_s = 0$, the e_x component and e_y component only have a $\pi/2$ phase difference ($\delta_{yx} = -\pi/2$), which means that the transverse component of the electric field is circularly polarized. In this case, the behavior of the SDVs is dependent on the Gouy phase difference δ_{xz} , and, in the monotonic interval of δ_{xz} , the special structure, ‘spiral SDVs’ (i.e., the SDVs rotate around the central axis), will be generated^[10,12]. The curves of δ_{xz} with different values of semi-aperture angle α are shown in Fig. 3. As one can see, the monotonic intervals of δ_{xz} are formed in each plot, and the range is increased with α , which is consistent with those observed in Ref. [10]. While the difference from that in Ref. [10] is that in Fig. 3(b), there exist two special points near $z_s = \pm 2.9\lambda$, and the δ_{xz} has a π phase jump at these two points. This

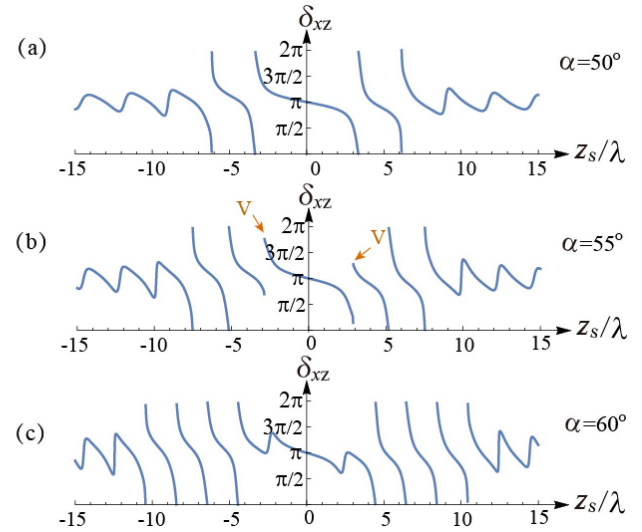


Fig. 3. Gouy phase difference δ_{xz} on the propagation axis with different semi-aperture angles. (a) $\alpha = 50^\circ$, (b) $\alpha = 55^\circ$, (c) $\alpha = 60^\circ$.

phenomenon is caused by the null SD at these two points, i.e., the ‘SDV singularity’^[14]. Note that the SDV singularity describes a point at which the SD is zero, the SDV is thus undefined, and the topological structure around this singularity follows the same rule as the traditional vector singularity of electric fields does.

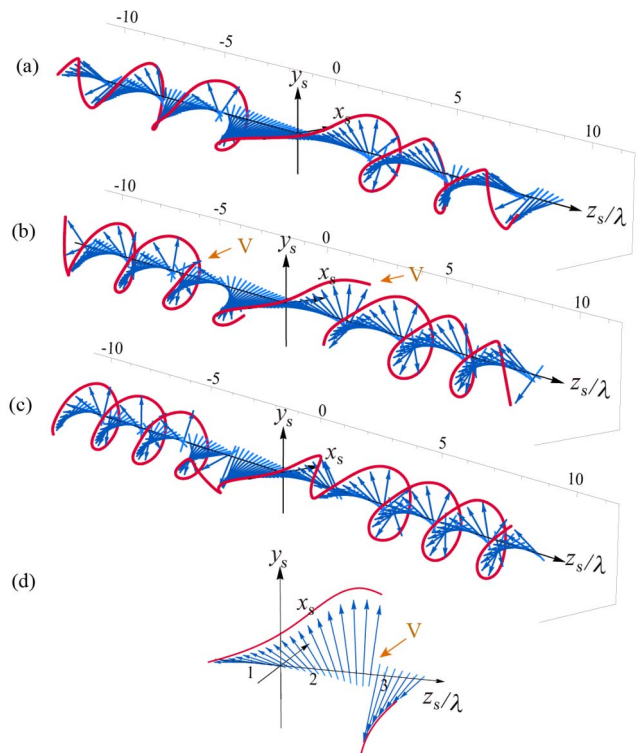


Fig. 4. SDVs on the propagation axis with different semi-aperture angles. (a) $\alpha = 50^\circ$, (b) $\alpha = 55^\circ$, (c) $\alpha = 60^\circ$, (d) SDVs near a SDV singularity in (b).

The corresponding SDVs on the z_s axis are illustrated in Fig. 4, where the blue arrows denote the SDVs and the red curve is their envelope. We can see that in the monotonic intervals of δ_{xz} [for instance $(-7\lambda, +7\lambda)$ in Fig. 4(b)], the SDVs rotate clockwise along the propagation axis, and, as α increases, the rotation range (corresponding to the monotonic interval in Fig. 3) expands [i.e., this range in Fig. 4(c) is bigger than that in Figs. 4(a) and 4(b)]. Especially, at the points with SDV singularity in Fig. 4(b) (denoted by ‘V’), the SDVs do not exist, while by passing through these points the SDVs reverse their directions. This is depicted more clearly in Fig. 4(d), where the SDVs at points $z_s = 2.8\lambda, 2.9\lambda$ have (nearly) opposite directions (note that the exact position of this singular point is between 2.8λ and 2.9λ).

Second, the SDVs exhibit special behaviors on the y_s axis. When $\phi_s = \pm\pi/2$, from Eqs. (3)–(19), we can obtain $\delta_{zy} = \pm\pi/2$, $\delta_{xz} = 0, \pm\pi$, and $\delta_{yx} = \pm\pi/2$, which means that here the Gouy phase differences are constants (their signs change at the points of phase singularity). This fact leads to $s_E^{(x)} = \pm C_0 |e_y| |e_z|$, $s_E^{(y)} = 0$, $s_E^{(z)} = \pm C_0 |e_x| |e_y|$ (here $C_0 = \epsilon_0/2\omega$). Therefore, along this axis all of the SDVs are exactly perpendicular to the y_s direction, and the SDV singularities can be observed easily. The Gouy phase differences δ_{zy} and δ_{yx} are shown in Fig. 5. One can see firstly that the values of δ_{zy} and δ_{yx} are very different on the $+y_s$ axis and the $-y_s$ axis, i.e., asymmetric with respect to the origin O . Second, δ_{zy} (or δ_{yx}) has a π jump at the phase singularities of the e_y or e_z component (or the e_x or e_y component). Also, δ_{zy} and δ_{yx} have their common ‘jump’ points, which can be seen along the dotted (vertical) lines in Fig. 5. At these common ‘jump’ points [denoted by ‘ V_i ’ ($i = 1, 2, \dots, 6$)], the SDV singularities are formed, which also can be observed in Fig. 6.

In Fig. 6, the SDVs with the same parameter as Fig. 5 are displayed [note that here the plots (a) and (b) are the same figure but seen from different views]. One can see firstly that all the SDVs are perpendicular to the y_s axis. Second, there are six ‘vector singularities’ from $y_s = -2.6\lambda$ to $y_s = +2.6\lambda$, and the SDVs have opposite directions at the two sides of each ‘vector singularity.’ Furthermore, the SDVs have quite different distributions on the two half-axes. This asymmetry is mainly caused by the

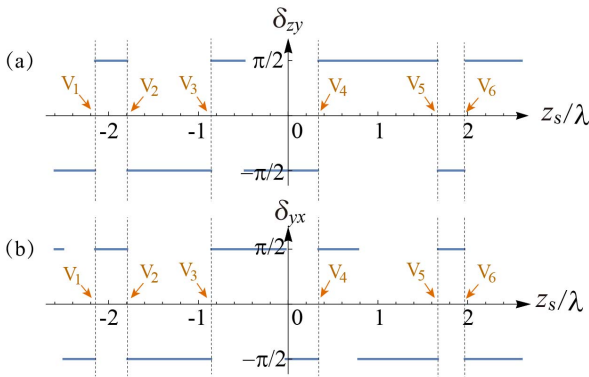


Fig. 5. Gouy phase differences δ_{zy} and δ_{yx} on the y_s axis: $\alpha = 60^\circ$.

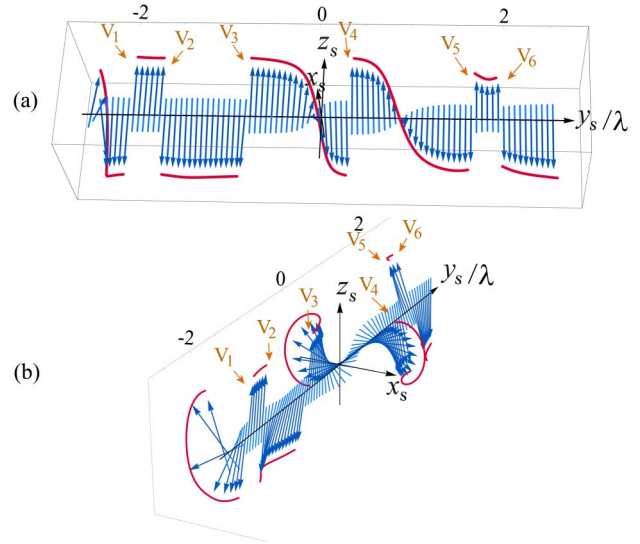


Fig. 6. SDVs on the y_s axis. (a) and (b) are the same figure from different views: $\alpha = 60^\circ$.

rotation of the spatial distribution of the SDVs, which will be discussed in the following part.

Third, the spatial distribution of the tSDVs rotates during beam propagation. The tSDVs, $s_E^{(t)} = (s_E^{(x)}, s_E^{(y)})$, in the focal plane are shown in Fig. 7(a), where the arrows denote the tSDVs with their size and color indicating the density of the tSDVs (i.e., the transverse SD). The color-coded transverse SD of the same region is also shown in Fig. 7(b). We can see that there are six strong density spots, and they are distributed symmetrically with respect to the y_s axis. The tSDVs on the transverse planes at different propagation distances are displayed in Fig. 8, from which one see that the spatial distribution of the tSDVs rotates clockwise as the beam propagates. To illustrate this rotation exactly, we selected two maxima density points denoted by a black circle and a black square, respectively (see Fig. 8), and their azimuthal angles at different transverse planes are plotted in Fig. 9.

From Fig. 9, we can find that the point denoted by the circle rotates from about 170° to 110° , and the other one circles from around 70° to 10° . Both total rotation angles are about 60° . This rotation can be explained by the difference of the general Gouy

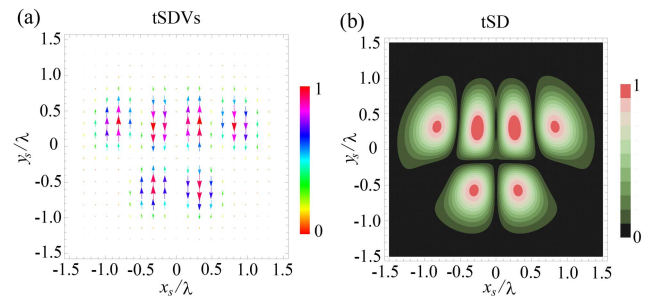


Fig. 7. (a) tSDVs and (b) transverse SDs on the focal plane.

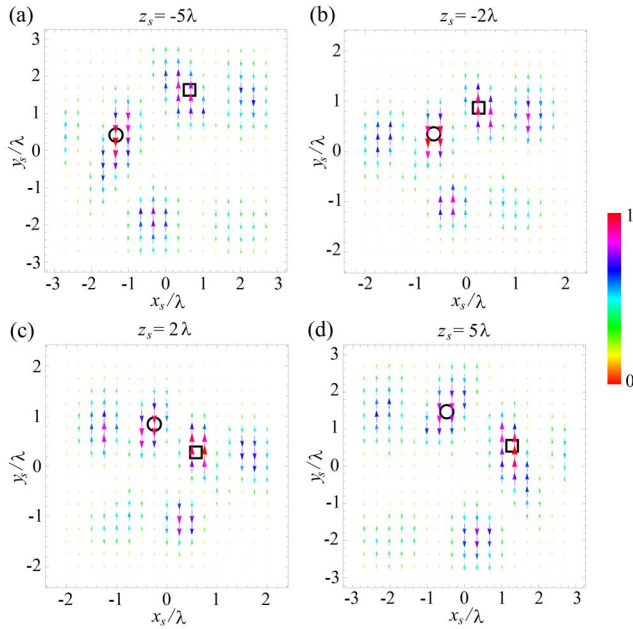


Fig. 8. tSDVs on selected transverse planes.

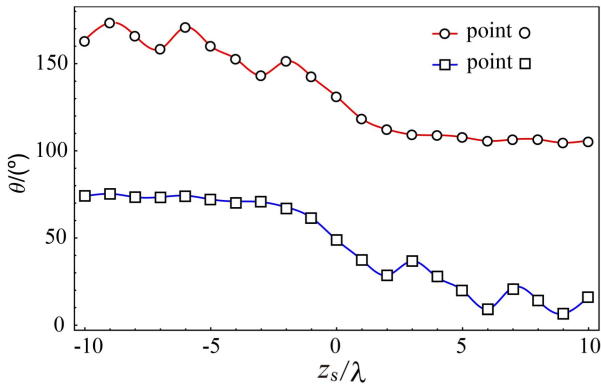


Fig. 9. Rotation angles of two maxima points of the transverse SD on the transverse planes from $z_s = -10\lambda$ to $z_s = +10\lambda$.

phases between two beams with different OAM modes. The incident field is composed by two beams with $t_1 = +1$ and $t_2 = -2$. As we discussed before, here, the general Gouy phases of these beams can be calculated from Eq. (21), and they are 2π and 3π . Due to this general Gouy phase difference, with the beam propagation, the composite field will acquire an angular change on the field distribution, and this change is $\frac{\pi(|t_2| - |t_1|)}{t_2 - t_1} = -\pi/3$ ^[22] (note that the value $-\pi/3$ is calculated for the beam propagating from $-\infty$ to $+\infty$). Therefore, the spatial distribution of the tSDVs gets an about 60° clockwise rotation.

4. Conclusions

In conclusion, the evolution of the SDVs of a strongly focused composite field is studied. It is found that in such a field, the

SDVs of the points on the z_s axis can rotate with the beam propagation, while the SDVs for the points on the y_s axis are all perpendicular to the y_s direction. These two phenomena can be explained by the Gouy phase difference between the field polarization components (i.e., the components with different polarization states). Particularly, the SDV singularities are also observed on these two axes, and the SDVs will reverse their directions by passing through these singularities. The spatial distribution of the tSDVs (the transverse component of SDVs) is examined, and it is found that the tSDVs' distribution will have a 60° rotation during the beam propagation. It is quite interesting to see that this 60° rotation is caused by the general Gouy phase difference between the field OAM modes (i.e., the components with different OAM modes) rather than the field polarization components. The findings in this Letter may have applications in optical manipulations; on the other hand, this work also supplies a simple model for observing rich behaviors of SDVs and for distinguishing two types of Gouy phases.

Acknowledgement

This work was supported by the National Natural Science Foundation of China (NSFC) (No. 11974281) and the Natural Science Basic Research Plan in Shaanxi Province of China (No. 2020JM-116).

References

1. K. Y. Bliokh, A. Y. Bekshaev, and F. Nori, "Extraordinary momentum and spin in evanescent waves," *Nat. Commun.* **5**, 3300 (2014).
2. T. Bauer, M. Neugebauer, G. Leuchs, and P. Banzer, "Optical polarization Möbius strips and points of purely transverse spin density," *Phys. Rev. Lett.* **117**, 013601 (2016).
3. C. Junge, D. O'Shea, J. Volz, and A. Rauschenbeutel, "Strong coupling between single atoms and nontransversal photons," *Phys. Rev. Lett.* **110**, 213604 (2013).
4. M. Neugebauer, T. Bauer, P. Banzer, and G. Leuchs, "Polarization tailored light driven directional optical nanobeacon," *Nano Lett.* **14**, 2546 (2014).
5. A. Aiello, N. Lindlein, C. Marquardt, and G. Leuchs, "Transverse angular momentum and geometric spin Hall effect of light," *Phys. Rev. Lett.* **103**, 100401 (2009).
6. J. Korger, A. Aiello, V. Chille, P. Banzer, C. Wittmann, N. Lindlein, C. Marquardt, and G. Leuchs, "Observation of the geometric spin Hall effect of light," *Phys. Rev. Lett.* **112**, 113902 (2014).
7. A. Aiello, P. Banzer, M. Neugebauer, and G. Leuchs, "From transverse angular momentum to photonic wheels," *Nat. Photon.* **9**, 789 (2015).
8. A. Aiello and P. Banzer, "The ubiquitous photonic wheel," *J. Opt.* **18**, 085605 (2016).
9. W. Miao, X. Pang, and W. Liu, "Photonic wheels and their topological reaction in a strongly focused amplitude tailored beam," *IEEE Photon. J.* **12**, 6500709 (2020).
10. X. Pang and W. Miao, "Spinning spin density vectors along the propagation direction," *Opt. Lett.* **43**, 4831 (2018).
11. J. S. Eismann, P. Banzer, and M. Neugebauer, "Spin-orbit coupling affecting the evolution of transverse spin," *Phys. Rev. Res.* **1**, 033143 (2019).
12. J. Zhuang, L. Zhang, and D. Deng, "Tight-focusing properties of linearly polarized circular Airy Gaussian vortex beam," *Opt. Lett.* **45**, 296 (2020).
13. Z. Man, X. Dou, and H. P. Urbach, "The evolutions of spin density and energy flux of strongly focused standard full Poincaré beams," *Opt. Commun.* **458**, 124790 (2020).

14. X. Pang, C. Feng, B. Nyamdorj, and X. Zhao, "Hidden singularities in 3D optical fields," *J. Opt.* **22**, 115605 (2020).
15. M. Born and E. Wolf, *Principles of Optics: Electromagnetic Theory of Propagation, Interference and Diffraction of Light* (Cambridge University, 1999).
16. T. D. Visser and E. Wolf, "The origin of the Gouy phase anomaly and its generalization to astigmatic wavefields," *Opt. Commun.* **283**, 3371 (2010).
17. M.-S. Kim, T. Scharf, C. Rockstuhl, and H. P. Herzig, "Phase anomalies in micro-optics," *Prog. Opt.* **58**, 115 (2013).
18. J. F. Federici, R. L. Wample, D. Rodriguez, and S. Mukherjee, "Application of terahertz Gouy phase shift from curved surfaces for estimation of crop yield," *Appl. Opt.* **48**, 1382 (2009).
19. X. Pang, D. G. Fischer, and T. D. Visser, "Wavefront spacing and Gouy phase in presence of primary spherical aberration," *Opt. Lett.* **39**, 88 (2014).
20. J. Zhang, X. Pang, and J. Ding, "Wavefront spacing and Gouy phase in strongly focused fields: the role of polarization," *J. Opt. Soc. Am. A* **34**, 1132 (2017).
21. L. Paterson, M. P. MacDonald, J. Arlt, W. Sibbett, P. E. Bryant, and K. Dholakia, "Controlled rotation of optically trapped microscopic particles," *Science* **292**, 912 (2001).
22. S. M. Baumann, D. M. Kalb, L. H. MacMillan, and E. J. Galvez, "Propagation dynamics of optical vortices due to Gouy phase," *Opt. Express* **17**, 9818 (2009).
23. A. Forbes, "Controlling light's helicity at the source: orbital angular momentum states from lasers," *Phil. Trans. R. Soc. A* **375**, 20150436 (2017).
24. S. Wei, D. Wang, J. Lin, and X. Yuan, "Demonstration of orbital angular momentum channel healing using a Fabry-Pérot cavity," *Opto-Electron Adv.* **1**, 180006 (2018).
25. X. Yang, S. Wei, S. Kou, F. Yuan, and E. Cheng, "Misalignment measurement of optical vortex beam in free space," *Chin. Opt. Lett.* **17**, 090604 (2019).
26. T. Lin, A. Liu, X. Zhang, H. Li, L. Wang, H. Han, Z. Chen, X. Liu, and H. Lü, "Analyzing OAM mode purity in optical fibers with CNN-based deep learning," *Chin. Opt. Lett.* **17**, 100603 (2019).
27. X. Yan, L. Guo, M. Cheng, and S. Chai, "Free-space propagation of autofocusing Airy vortex beams with controllable intensity gradients," *Chin. Opt. Lett.* **17**, 040101 (2019).
28. G. Indebetouw, "Optical vortices and their propagation," *J. Mod. Opt.* **40**, 73 (1993).
29. B. Richards and E. Wolf, "Electromagnetic diffraction in optical systems. II. Structure of the image field in an aplanatic system," *Proc. R. Soc. A* **253**, 358 (1959).